

Variational data assimilation for tropospheric chemistry modeling

Hendrik Elbern, Hauke Schmidt, and Adolf Ebel

Institute for Geophysics and Meteorology, University of Cologne, Germany

Abstract. The method of variational adjoint data assimilation has been applied to assimilate chemistry observations into a comprehensive tropospheric gas phase model. The rationale of this method is to find the correct initial values for a subsequent atmospheric chemistry model run when observations scattered in time are available. The variational adjoint technique is esteemed to be a promising tool for future advanced meteorological forecasting. The stimulating experience gained with the application of four-dimensional variational data assimilation in this research area has motivated the attempt to apply the technique to air quality modeling and analysis of the chemical state of the atmosphere. The present study describes the development and application of the adjoint of the second generation regional acid deposition model gas phase mechanism, which is used in the European air pollution dispersion model system. Performance results of the assimilation scheme using both model-generated data and real observations are presented for tropospheric conditions. In the former case it is demonstrated that time series of only few or even one measured key species convey sufficient information to improve considerably the analysis of unobserved species which are directly coupled with the observed species. In the latter case a Lagrangian approach is adopted where trajectory calculations between two comprehensively furnished measurement sites are carried out. The method allows us to analyze initial data for air pollution modeling even when only sparse observations are available. Besides remarkable improvements of the model performance by properly analyzed initial concentrations, it is shown that the adjoint algorithm offers the feasibility to estimate the sensitivity of ozone concentrations relative to its precursors.

1. Introduction

Atmospheric chemistry models as solvers of an initial-boundary value problem generally call for the provision of pertinent initial values. Unlike in meteorological forecasting, the question of finding the correct initial values with the aid of observations, that is, the data assimilation problem, has attracted only minor attention until now.

Two deciding factors may have hampered efforts in analyzing chemical trace species analogous to meteorological forecasting: (1) measurement sites of chemical constituents are very sparse in comparison with the well established synoptic observation networks of meteorological parameters, and (2) chemistry-transport simulations are often esteemed to be controlled to a large extent by emission and deposition processes, rather than by initial values.

Therefore, in many applications of limited area chemistry models, special care is only taken to place model boundaries sufficiently far windward from regions with enhanced anthropogenic emissions, which then are most carefully estimated. By this, model domains are selected to encompass the areas with the decisive chemical and physical processes of interest and the model concentrations are then assumed to enter realistic levels after a certain runtime. In the regional acid deposition model (RADM), after a spin-off run of a few days, which is started with clean background conditions, initial values are provided for the simulation of the subsequent episode of interest [Chang *et al.*, 1987]. With this approach it is tacitly assumed that the model state is attracted to the real state to a sufficiently realistic degree. However, this is not a strictly well-founded assumption.

Conditions (1) and (2) mentioned above hold to a far lesser extent in the stratosphere, where satellite data may provide a better observation density compared with surface measurements and emissions are restricted to high-flying aircraft exhaust in the flight corridors of the lowest stratosphere. Consequently, up to now, studies on chemical data assimilation using an ad-

vanced space-time approach have been devoted to the stratosphere only.

In early studies, *Salby* [1982a, b] provided an interpolation scheme for synoptic satellite observations. *Austin* [1992] proposed a model based analysis method where limb infrared monitor of the stratosphere (LIMS) satellite data were assimilated into a 30 day simulation run. LIMS observations of ozone, nitric acid, nitrogen dioxides, and water vapor were nudged into the model by introducing suitably defined weights and the resulting analyses appeared to be in good agreement with independently mapped archived data.

However, the nudging approach suffers from two principal detriments: (1) Insertion of observations into the model generally drives the state variables away from their status near to chemical equilibrium. The ensuing relaxation does not necessarily leave the observed species close to their measured concentration levels. (2) No direct use is made of available knowledge inherent in chemical mechanisms as comprised in comprehensive models, which would ensure that nonobserved species have concentration levels consistent with the respective measurements. A given time series can only be used by single observations rather than by its temporal evolution and tendencies. Therefore a long assimilation interval with a huge set of measured data is prerequisite but not sufficient for a moderate improvement of an analysis. A theoretical appreciation of these facts is given by *Bennett* [1992, section 4.3], who demonstrated that only a comprehensive and high quality data set may have a beneficial impact with the nudging method.

In the mid 1980s a completely different approach of assimilation for meteorological observations was introduced by *Lewis and Derber* [1985], *Le Dimet and Talagrand* [1986], and *Talagrand and Courtier* [1987], where fundamental ideas of the "optimum control" theory were introduced. Taking the initial values as "control parameters," a scalar "distance function" is defined, which provides a measure of weighted and accumulated distances between available observations and the values of the corresponding state variables predicted by models during a predefined "assimilation window." The minimization procedure of the distance function requires the knowledge of the local gradient with respect to the initial state, which is supplied by the adjoint of the tangent linear version of the model. The procedure is commonly referred to as four-dimensional variational data assimilation (4D-var). Due to its considerable computational expenditure, this method is presently implemented only in preoperational versions at weather centers [*Parrish and Derber*, 1992; *Courtier et al.*, 1994].

In stratospheric chemistry simulations the concept of variational data assimilation was first introduced by *Fisher and Lary* [1995], who developed the adjoint of a reduced gas phase mechanism for the stratosphere and combined chemistry with isentropic trajectory calculations. In the present study the adjoint of the second-generation regional acid deposition model (RADM2)

gas phase mechanism [*Stockwell et al.*, 1990] is developed. It is the intention in the paper to give an account of the prospects and limits of a variational data assimilation approach applied to a comprehensive and well-established gas phase mechanism, which is designed for use in mesoscale Eulerian tropospheric air quality models such as the European air pollution dispersion model (EURAD) [*Hass et al.*, 1995]. Also unlike *Fisher and Lary* [1995], the assimilation concept invoked here is based on a very limited data assimilation window of some hours only, to predict the chemical state of the atmosphere subsequent to this analysis interval. It is noted in passing that the term "initialization," which denotes the filtering of numerically induced spurious inertia-gravity waves in meteorological models, is intentionally rejected to avoid confusion.

The basics of adjoint theory and modeling are outlined in section 2. Some principal details of the RADM2 gas phase mechanism are given in section 3. In section 4, tests of the variational adjoint assimilation method with artificial observations are described. The subsequent exposition in section 5 is concerned with real data obtained from a measurement campaign. In section 6 the results are discussed, and suggestions for further work are given.

2. Variational Data Assimilation With the Adjoint Technique

In this study the initial value problem of a chemistry forecast model is addressed, which means to find initial concentrations, such that an optimal fit to observed concentrations, scattered in time, is achieved. The optimal estimation of emission and deposition rates, internal model parameters, or even meteorological parameters are conceptually related problems, but are not the subject of this paper.

The optimization problem may be condensed in a suitably defined distance function $\mathcal{J}(\mathbf{x}(t))$ which is a measure of the model's predictive skill with respect to observations. The scalar function $\mathcal{J}(\mathbf{x}(t))$ is to be minimized, where $\mathbf{x}(t)$ is the vector valued state variable of the model, which, in our case, is the vector with the species' concentration levels. A coarse outline of the procedure reads as follows: (1) find the gradient $\nabla_{\mathbf{x}(t_0)}\mathcal{J}$ of the distance function, and (2) find $\mathbf{x}^{n+1}(t_0)$, $n = 0, 1, \dots$ such that $\mathcal{J}(\mathbf{x}^{n+1}(t_0)) < \mathcal{J}(\mathbf{x}^n(t_0))$, with the aid of $\nabla_{\mathbf{x}(t_0)}\mathcal{J}$ and previously calculated gradients. (3) Repeat this sequence until \mathcal{J} becomes smaller than a prescribed threshold value.

2.1. Adjoint Computation of $\nabla_{\mathbf{x}(t_0)}\mathcal{J}$

For the sake of completeness and later notational reference, we will briefly outline the approach that provides the gradient of the distance function by means of the adjoint calculus. A mathematically strict and comprehensive derivation is dealt with by *Talagrand and*

Courtier [1987, and references therein]. The cursory survey here mainly follows this study.

The distance function \mathcal{J} may be defined as follows:

$$\mathcal{J}(\mathbf{x}(t)) = \frac{1}{2}(\mathbf{x}_b - \mathbf{x}(t_0))^T \mathbf{B}^{-1}(\mathbf{x}_b - \mathbf{x}(t_0)) + \frac{1}{2} \int_{t_0}^{t_N} (\hat{\mathbf{x}}(t) - \mathbf{x}(t))^T \mathbf{O}^{-1}(\hat{\mathbf{x}}(t) - \mathbf{x}(t)) dt \quad (1)$$

where \mathcal{J} is a scalar functional defined on the time interval $t_0 \leq t \leq t_N$ dependent on the vector valued state variable $\mathbf{x} \in \mathcal{H}$ with \mathcal{H} denoting a Hilbert space. The first guess or background values \mathbf{x}_b are defined at $t = t_0$, and \mathbf{B} is the covariance matrix of the estimated background error. The observations are denoted $\hat{\mathbf{x}}$ and the observation and representativeness errors are included in the covariance matrix \mathbf{O}^{-1} . For simplicity we assume direct observations of the model's state variables.

Let the differential equation of the model \mathbf{M} be given by

$$\frac{d\mathbf{x}}{dt} = \mathbf{M}(\mathbf{x}), \quad (2)$$

where \mathbf{M} acts as a generally nonlinear operator defining uniquely the state variable $\mathbf{x}(t)$ at time t , after an initial state $\mathbf{x}(t_0)$ is provided. The linear perturbation equation, giving the evolution of a small deviation $\delta\mathbf{x}(t)$ from a model state $\mathbf{x}(t)$ then reads

$$\frac{d\delta\mathbf{x}}{dt} = \mathbf{M}'\delta\mathbf{x}, \quad (3)$$

where \mathbf{M}' is the tangent linear model of \mathbf{M} . Denoting the inner product of \mathcal{H} by angle brackets, the operator \mathbf{M}' , mapping from \mathcal{H} into \mathcal{H} itself, has the adjoint operator \mathbf{M}'^* , which is defined by $\langle \mathbf{y}, \mathbf{M}'\mathbf{z} \rangle = \langle \mathbf{M}'^*\mathbf{y}, \mathbf{z} \rangle$ for all $\mathbf{y}, \mathbf{z} \in \mathcal{H}$. For the remainder we drop the background term in (1) but we introduce the model (2) as a strong constraint with Lagrange multipliers $\lambda(t)$. Setting $1/2 (\hat{\mathbf{x}}(t) - \mathbf{x}(t))^T \mathbf{O}^{-1}(\hat{\mathbf{x}}(t) - \mathbf{x}(t)) = \mathcal{O}(t)$ for notational convenience, (1) then reads

$$\mathcal{J}(\mathbf{x}(t)) = \int_{t_0}^{t_N} \mathcal{O}(t) + \langle \lambda, \frac{d\mathbf{x}(t)}{dt} - \mathbf{M}\mathbf{x}(t) \rangle dt. \quad (4)$$

Then, the variation of the distance function $\mathcal{J}(\mathbf{x}(t_0))$ can be expressed as

$$\begin{aligned} \delta\mathcal{J} &= \int_{t_0}^{t_N} \left(\langle \nabla_{\mathbf{x}} \mathcal{O}(t), \delta\mathbf{x}(t) \rangle + \langle \delta\lambda, \frac{d\mathbf{x}(t)}{dt} - \mathbf{M}\mathbf{x}(t) \rangle \right. \\ &\quad \left. + \langle \lambda, \frac{d\delta\mathbf{x}(t)}{dt} - \mathbf{M}'\delta\mathbf{x}(t) \rangle \right) dt \\ &= \int_{t_0}^{t_N} \left(\langle \nabla_{\mathbf{x}} \mathcal{O}(t) - \frac{d\lambda(t)}{dt} - \mathbf{M}'^*\lambda(t), \delta\mathbf{x}(t) \rangle \right. \\ &\quad \left. + \langle \delta\lambda, \frac{d\mathbf{x}(t)}{dt} - \mathbf{M}\mathbf{x}(t) \rangle \right) dt \\ &\quad + \lambda(t_N)\delta\mathbf{x}(t_N) - \lambda(t_0)\delta\mathbf{x}(t_0), \end{aligned} \quad (5)$$

where integration by parts was applied. Introducing the

extremal principle $\delta\mathcal{J} = 0$, the integrand includes the inhomogeneous adjoint equation, which is forced by the observation term on the right-hand side of (6) at time t

$$-\frac{d\lambda(t)}{dt} - \mathbf{M}'^*\lambda(t) = \mathbf{O}^{-1}(\hat{\mathbf{x}}(t) - \mathbf{x}(t)). \quad (6)$$

The integration of the tangent linear equation (3) gives the evolution of an initial perturbation $\delta\mathbf{x}(t_0)$ at later times t_n and can formally be expressed as

$$\delta\mathbf{x}(t_n) = \mathbf{R}(t_n, t_0)\delta\mathbf{x}(t_0), \quad (7)$$

where the operator $\mathbf{R}(t_n, t_0)$ denotes the resolvent of \mathbf{M}' for the time interval $[t_0, t_n]$ acting on the initial state $\mathbf{x}(t_0)$.

Since (7) generally admits only of numerical solution, $\delta\mathbf{x}(t_n)$ may be approximated by the sequence

$$\delta\mathbf{x}(t_n) = \tilde{\mathbf{R}}(t_n, t_{n-1})\tilde{\mathbf{R}}(t_{n-1}, t_{n-2}) \dots \tilde{\mathbf{R}}(t_1, t_0)\delta\mathbf{x}(t_0) \quad (8)$$

with $\tilde{\mathbf{R}}(t_i, t_{i-1})$ being a sufficiently accurate numerical operator for the stepwise integration of (3).

Designating \mathbf{S} as the resolvent of \mathbf{M}'^* , it can be shown that $\mathbf{S}(t_i, t_j)$ is the adjoint of $\mathbf{R}(t_j, t_i)$, or, for any $\delta\mathbf{x}, \lambda$, we have $\langle \lambda(t_N), \mathbf{R}(t_N, t_0)\delta\mathbf{x}(t_0) \rangle = \langle \mathbf{S}(t_0, t_N)\lambda(t_N), \delta\mathbf{x}(t_0) \rangle$. This is readily seen from the conservation of the inner product of a perturbed state variable $\delta\mathbf{x}(t)$ and its adjoint $\lambda(t)$, if external forcing in (6) is excluded:

$$\frac{d}{dt} \langle \lambda(t), \delta\mathbf{x}(t) \rangle = \langle \lambda(t), \mathbf{M}'\delta\mathbf{x}(t) \rangle - \langle \mathbf{M}'^*\lambda(t), \delta\mathbf{x}(t) \rangle = 0. \quad (9)$$

With the aid of (5) and (7) it is now possible to express $\delta\mathcal{J}$ as a function of $\mathbf{x}(t_0)$ alone

$$\begin{aligned} \delta\mathcal{J}(\mathbf{x}(t_0)) &= \int_{t_0}^{t_N} \langle \nabla_{\mathbf{x}} \mathcal{O}(t), \mathbf{R}(t, t_0)\delta\mathbf{x}(t_0) \rangle dt \\ &= \langle \int_{t_0}^{t_N} \mathbf{S}(t_0, t) \nabla_{\mathbf{x}} \mathcal{O}(t) dt, \delta\mathbf{x}(t_0) \rangle, \end{aligned} \quad (10)$$

which finally leads to the desired gradient of \mathcal{J} , given in terms of a discretized expression of the adjoint operator $\mathbf{S}(t_0, t)$

$$\nabla_{\mathbf{x}(t_0)} \mathcal{J} = \sum_{m=0}^N \tilde{\mathbf{S}}(t_0, t_1) \tilde{\mathbf{S}}(t_1, t_2) \dots \tilde{\mathbf{S}}(t_{m-1}, t_m) \nabla_{\mathbf{x}} \mathcal{O}(t_m). \quad (11)$$

It remains to be shown that $\nabla_{\mathbf{x}(t_0)} \mathcal{J} = \lambda(t_0)$. Defining the backward initial condition $\lambda(t_N) = 0$ and given a single instantaneous forcing $\hat{\lambda}(t') = -\nabla_{\mathbf{x}(t')} \mathcal{O}(t')$ at any time t' , $t \leq t' < t_N$, (6) may be rewritten, again in exact form for convenience, as

$$\begin{aligned} \frac{\partial}{\partial t} \mathbf{S}(t, t') \nabla_{\mathbf{x}(t')} \mathcal{O}(t') &= -\frac{d\hat{\lambda}(t)}{dt} \\ &= -\mathbf{M}'^* \mathbf{S}(t, t') \nabla_{\mathbf{x}(t')} \mathcal{O}(t'), \end{aligned} \quad (12)$$

to reveal that $\frac{\partial}{\partial t} \mathbf{S}(t, t') = -\mathbf{M}'^* \mathbf{S}(t, t')$.

Integration of (12) then gives

$$\hat{\lambda}(t) = \mathbf{S}(t, t') \nabla_{\mathbf{x}(t')} \mathcal{O}(t'). \quad (13)$$

Since the resolvent \mathbf{S} is a linear operator, all observations can be combined by adding up the corresponding equations (13), which demonstrates the proposition for $t = t_0$.

The computational procedure to calculate the gradient $\nabla_{\mathbf{x}(t_0)} \mathcal{J}$ is first to integrate "forward in time" the "forward" model \mathbf{M} by (2), followed by an integration "backward in time" of the adjoint ("backward") equation (11). The forward integration provides the distance function value $\mathcal{J}(\mathbf{x}(t_0))$ and intermediate values for retrieving the operators \mathbf{S} for the backward integration, while the backward integration gives the gradient $\nabla_{\mathbf{x}(t_0)} \mathcal{J}$. Both \mathcal{J} and $\nabla_{\mathbf{x}(t_0)} \mathcal{J}$ values then enter the minimization routine.

2.2. Minimization Algorithm

Zou *et al.* [1993a] identified the Broyden–Fletcher–Goldfarb–Shanno (BFGS) algorithm in its limited memory version as a recommendable implementation of the quasi-Newton minimization method for large-scale atmospheric optimization problems. Anticipating later spatial extensions, a basic version of the algorithm was used to solve the minimization problem of the distance function.

However, unlike in meteorological applications, the minimization is constrained due to the positive definiteness of chemical species as the control variables in the present study. Following a method proposed by Bertsekas [1982], the off-diagonal elements in the approximation to the inverse Hessian matrix of rows and columns of species with very low concentrations were set to 0. This procedure inhibits the resulting direction vector to point toward a virtual global minimum beyond the constraint boundary. Rather, the direction toward the minimum along the constraining boundary is given. The preconditioning follows Navon *et al.* [1992] and only consists of a multiplication of a diagonal matrix with the vector of initial concentrations. The elements of the matrix are defined to be the inverses of the first guess concentrations. Therefore the preconditioning method chosen here is a computationally very cheap operation.

An additional limited memory BFGS algorithm for constrained problems [Byrd *et al.*, 1994] is implemented for comparison. This algorithm shows a similar performance as the method of Bertsekas but is expected to be superior in the case of later dimensional extension of the model.

2.3. Adjoint of the Chemistry Equations

The model \mathbf{M} in the present study is the ordinary differential equation system for gas phase chemistry.

Considering elementary gas phase reactions [Finlayson–Pitts and Pitts, 1986], the set of ordinary differential equations for U species may be combined to give

$$\frac{dx_i}{dt} = \sum_{r=1}^R \left(k(r) (s_i(r_+) - s_i(r_-)) \prod_{j=1}^U x_j^{s_j(r_-)} \right), \quad i = 1, \dots, U. \quad (14)$$

Here the rate of concentration change of species x_i is governed by R reactions with reaction rates $k(r)$. The stoichiometric coefficient $s \in \mathbb{N}_0$ of species l appearing on the product side (+) or educt side (−) in reaction r is designated $s_l(r_{\pm})$, respectively. Comprising unimolecular, bimolecular, and termolecular reactions, the stoichiometric coefficients obey the inequality $\sum_{j=1}^U s_j(r_{\pm}) \leq 3$.

After performing the necessary specific manipulations analogous to (5) we find the adjoint equation of (14)

$$\frac{d\lambda_i}{dt} = - \sum_{r=1}^R \left(k(r) \frac{s_i(r_-)}{x_i} \prod_{j=1}^U x_j^{s_j(r_-)} \times \sum_{n=1}^U (s_n(r_+) - s_n(r_-)) \lambda_n \right), \quad i = 1, \dots, U. \quad (15)$$

It is noted in passing that the developed adjoint code of the gas phase mechanism is not based on (15). Rather, the technique of adjoining line by line from the forward code is adopted in this study.

2.4. On the Ambiguity of the Assimilation Result

From a theoretical viewpoint it is now briefly considered to what extent measurements of a limited set of species can reduce the manifold of possible initial perturbations $\delta \mathbf{x}(t_0)$ to fit to the observations. Without loss of generality, let there be observations of species $1, \dots, g$ out of $U \geq g$, all available at N observation times spread over the assimilation interval. Applying the resolvent $\tilde{\mathbf{R}}(t_n, t_{n-1})$ and truncating the lines of unobserved species, the linear system (8) then yields, with the aid of the measurement deviations $\delta \hat{x}_i(t_n) = \hat{x}_i(t_n) - x_i(t_n)$, $n = 1, \dots, N$, $i = 1, \dots, g$, N systems of linear equations

$$\begin{pmatrix} \delta \hat{x}_1(t_n) \\ \delta \hat{x}_2(t_n) \\ \vdots \\ \delta \hat{x}_g(t_n) \end{pmatrix} = [\mathbf{I}, \mathbf{0}] \tilde{\mathbf{R}}(t_n, t_{n-1}) \dots \tilde{\mathbf{R}}(t_1, t_0) \delta \mathbf{x}(t_0), \quad n = 1, \dots, N. \quad (16)$$

Here $[\mathbf{I}, \mathbf{0}]^{g \times U}$ is the truncation operator composed by the identity matrix $\mathbf{I}^{g \times g}$ and the zero matrix $\mathbf{0}^{g \times (U-g)}$. The resolvent operators $\tilde{\mathbf{R}}$ and the truncation operator are comprised in matrix $\mathcal{R}^{Ng \times U}$ for convenience

$$\begin{pmatrix} \delta \hat{\mathbf{x}}(t_1) \\ \delta \hat{\mathbf{x}}(t_2) \\ \vdots \\ \delta \hat{\mathbf{x}}(t_N) \end{pmatrix} = \mathcal{R}^{Ng \times U} \delta \mathbf{x}(t_0),$$

$$\begin{pmatrix} \delta \hat{\mathbf{x}}(t_1) \\ \delta \hat{\mathbf{x}}(t_2) \\ \vdots \\ \delta \hat{\mathbf{x}}(t_N) \end{pmatrix} \in \mathbb{R}^{Ng}, \delta \mathbf{x}(t_0) \in \mathbb{R}^U. \quad (17)$$

The system is underdetermined for $Ng < U$, or for $(Ng = U) \wedge (\mathcal{R}^{Ng \times U} \text{ being singular})$. Otherwise, for $Ng = U$ the system is uniquely determined. For $Ng > U$ the system is possibly overdetermined. In the latter case the condition number $\text{cond}(\mathcal{R}^{U \times U})$ of $\mathcal{R}^{U \times U}$ with any combination $mg_i = U$ can give an estimate of what beneficial impact may be expected from the assimilation of the selected species i and m observation times. In practice, all information is introduced. However, the condition number may provide some evidence of reasonable weighting of the observation.

With respect to the highly nonlinear character of (14), at least a highly ranked matrix \mathcal{R} can be expected if numerous observation times are available. This is possibly sustained by the variability of $k(r)$ due to temperature and insolation changes during the assimilation interval.

3. RADM2 Gas Phase Mechanism

In this study the gas phase mechanism of the second-generation regional acid deposition model (RADM2) as an approved state-of-the-art chemistry algorithm is adopted as forward model. A comprehensive description is provided by *Stockwell et al.* [1990]. For convenience we briefly summarize some principal features of the model only to the extent needed for elaborating further on particular aspects encountered in the ensuing sections.

RADM2 is an upgrade of its predecessor RADM1 mainly in terms of a more detailed treatment of the organic chemistry. The natural variety of organic species generally calls for an algorithmic simplification. To this end a reactivity lumped molecular approach is selected as adequate technique [*Stockwell*, 1986]. The chemical mechanism has 157 gas phase reactions with 63 model species, a breakdown of which reads as follows: 40 species are prognosed and their initial values are to be determined, that means, for the entire study holds $U = 40$. Seventeen species are diagnosed by algebraic relations, two species only appear as products and are further ignored due to their chemical inertia, while four species are kept constant. The prognosed species divide into 14 inorganic species and 26 organic species. From the latter, nine species are represented individually, whereas 17 classes are defined to realize the reactiv-

ity lumped molecular approach. Twentyone reactions are photolytic destructions.

The solution of the ordinary differential equation system (ODE), which is defined by the gas phase mechanism, is a set of highly nonlinear functions with respect to emitted species and initial values of the modeled species. ODEs of chemical kinetics are known to be stiff systems for which sophisticated multistep solvers impose impractically high storage requirements for a full three-dimensional model. *Chang et al.* [1987] used a mathematically less rigorous but more efficient method with respect to computation time and memory demands. The results agree quite satisfactorily with results obtained from the [*Gear*, 1971] scheme, which is a frequently used advanced multistep solver for reference purposes. To reduce the stiffness of the ODE system the pseudo- or quasi-steady-state approximation is applied, the benefit of which is advocated by several studies, for example, by *Hov et al.* [1989]. This method still proves to be competitive with more advanced ODE solvers when used in three-dimensional mesoscale models with fine resolution and frequent restart intervals [*Sandu et al.*, 1996]. Suitable linear combinations of chemical reactions with rapid chemical interchanges allow for an extension of the temporal step sizes. The implementation taken for this study is based on the coupling of four pairs of species: $\{\text{NO}, \text{NO}_2\}$, $\{\text{HO}, \text{HO}_2\}$, $\{\text{N}_2\text{O}_5, \text{NO}_3\}$, $\{\text{PAN}, \text{acetylperoxy radical}\}$.

For most of the reactions the model version of the present study takes a semi-implicit difference form, where the exponential function is approximated by the first two terms of the Taylor series. With C_i^t being the concentration of the i th species at time t , the production term for the i th species given by $P_i = \sum_{r=1}^R k(r) s_i(r_+) \prod_{j=1}^U x_j^{s_j(r_+)}$, and the destruction term $L_i = \sum_{r=1}^R k(r) s_i(r_-) \prod_{j=1}^U x_j^{s_j(r_-)}$, the algorithm then reads

$$C_i^{t+\Delta t_c} = \frac{\Delta t_c P_i^t + C_i^t - (\Delta t_c/2) L_i^t}{1 + (\Delta t_c/2)(L_i^t/C_i^t)}, \quad i = 1, \dots, U \quad (18)$$

where Δt_c is the variable time step of the algorithm. The calculation of Δt_c follows *McRae et al.* [1982] with a limited set of species selected to determine the time step. By practical reasons a lower bound is defined to be 1/1000 min.

The adjoint of the chemical reaction solver has not been coded starting from (18). Rather, it proved to be more practical to adjoin the forward code backwards line by line, as described for example by *Chao and Chang* [1992]. This approach is also common practice in developing adjoint codes for meteorological models until now.

An important component of the gas phase mechanism is the solver of the radiative transfer equation which provides the photolysis rates. In this study the radiation scheme of *Madronich* [1987] is applied.

4. Identical Twin Experiments

4.1. General Remarks

After developing the adjoint of the RADM2 gas phase mechanism, the algorithmic correctness of the code has been verified by “identical twin experiments.” This test concept invokes the perfect model assumption where a preceding forward model run artificially generates “observations.” For the verification of the adjoint code a dense subset of the generated “observations” can be provided for the assimilation algorithm, which then should manage to approximate the initial state of the “observation run” arbitrarily well within a due number of iterations.

On successful completion of this test phase, identical twin experiments can also be applied to explore the potential of the variational data assimilation method to cope with only sparsely available measurements, both in terms of temporal data gaps and limited sets of measured trace species, that is, N is small and $g \ll U$. However, it should be noted, that performance results of identical twin experiments may be too optimistic, when compared with later real world applications [Daley, 1991]. The extent of this overestimation must be expected to be related to an overall model deficiency.

The following identical twin experiments roughly present chemical conditions of an urban plume scenario in some distance from emission sources. Mixing and deposition processes are omitted as well. Pressure and temperature are kept constant with 1013 hPa and 298 K, respectively. As a consequence of subsection 2.4, a successful analysis mandates to look for an assimilation window embracing a nonlinear variation of the state variables. Hence the assimilation interval is selected to embrace dawn, starting at 0300 local time (LT) and ending at 0800 LT. Photolysis rates commence to increase from 0 at 0330 LT.

4.2. Assimilation of Continuous Short Term Ozone Measurements

Ozone is the most densely measured trace gas, and observation frequency is often high. Therefore the key

problem is the analysis and prediction of chemical conditions during the ensuing day while only ozone observations during a time window of a few hours are available. The first identical twin experiment addresses the questions: (1) Is the 4D-var assimilation procedure capable to reproduce an “error free measured” time series of ozone, and (2) which other trace species are linked with ozone by chemical kinetics closely enough to allow for an analysis of comparable skill?

From the output of a preceding “observation run” only a time series of ozone concentrations with a frequency of 5 min is extracted for the local time interval from 0300 to 0800 LT as assimilation window. This gives $N = 60$ and $g = 1$.

For the subsequent assimilation runs pressure, temperature, radiative condition and concentrations of the four constant model species are the same as in the observation run. Unlike ozone, where the initial value is taken from the first “measurement” of the time series, all other first guess values are arbitrarily set to be 400, 5, 0.5, 0.01 or 10^{-3} parts per billion by volume (ppbv), only fitting the observation run values by the respective order of magnitude. A rough climatological knowledge of the magnitude of trace species is thereby provided to the assimilation procedure. The values actually taken and the performance of the assimilation method are displayed for ozone in Figure 1 and for eight other constituents in Figure 2. In both figures the graphs of the first guess run are shown by dotted lines and the solid lines denote the result of the assimilation procedure. The forecast stops at 2400 LT. For success control the “ozone measurements” and the observation run curves are given by squares and dashed lines, respectively. It can be clearly seen that the first guess run and the “observation” run depart considerably in the last hour of the assimilation window at 0800 LT.

As can be seen from Figure 1, the forecasting skill for ozone is fully satisfying due to the assimilation of its observations. The same is true for the performance of the assimilation procedure in analyzing nonmeasured NO_x concentrations, which is mainly based on the close chemical kinetic links between photolysis of NO_2 and

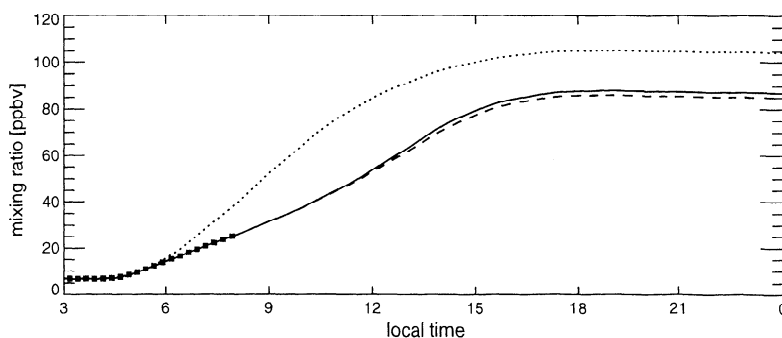


Figure 1. Assimilation of ozone and forecast until midnight with a 5 hour assimilation window spanning dawn. Every third model-generated ozone “measurement” is indicated by squares. Sunrise starts at about 0400 LT. The graph of the first guess run is given by a dotted line, the final assimilation run is given by a solid line. The control run is depicted by dashed lines.

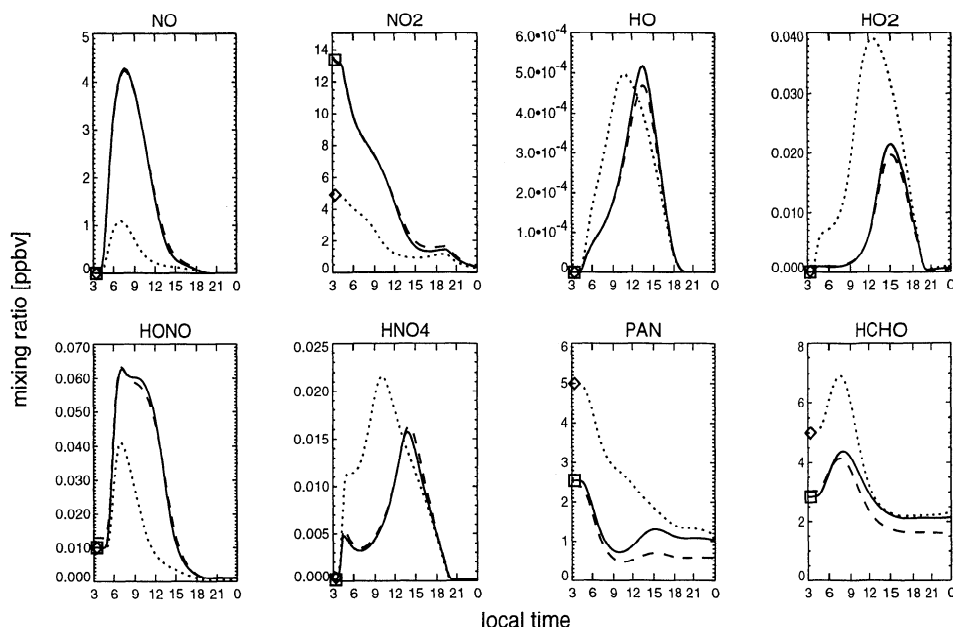


Figure 2. Analysis results for “unobserved” species of the same case as in Figure 1. Dotted lines give the first guess run; solid lines give the final assimilation run. The “true” values defined by the “observation” run are shown by dashed lines.

production of O_3 , and its destruction by reaction with NO (Figure 2). Following Altshuller [1983] the formation and destruction of PAN bears resemblance to the ozone concentration in the boundary layer which explains its successful analysis in the first half of the simulation interval (Figure 2). During later hours, however, the simulation skill diminishes probably due to missing observations of volatile organic compounds (VOC). Nevertheless, further success can be claimed for the analysis of the following species (Figure 2): HO and HO_2 are strongly involved in ozone formation and destruction; formaldehyde is indirectly linked with ozone via its photolysis to hydroperoxy radicals; the analysis of HNO_4 is based on the successful analysis of HO_2 and NO_2 which are direct precursors; HNO_2 , where the satisfying skill of the analysis is based on the reaction of OH and NO. It can be concluded that for species mentioned so far ozone is a key constituent which is able to determine their concentrations to a large degree during and beyond the assimilation interval. For other species of the RADM model a comparable success cannot be claimed. This does not at all imply that contributions to the ozone formation cannot be captured by the variational adjoint method. Rather, it appears to happen that these nonanalyzed species, which are mainly VOC, may adjust and substitute each other to attain the required total photolytical ozone creation potential as an ensemble. In fact, further test calculations, which are omitted for brevity, show that the addition of even sparse measurements of an arbitrary hydrocarbon is sufficient for a satisfying analysis of the constituent observed.

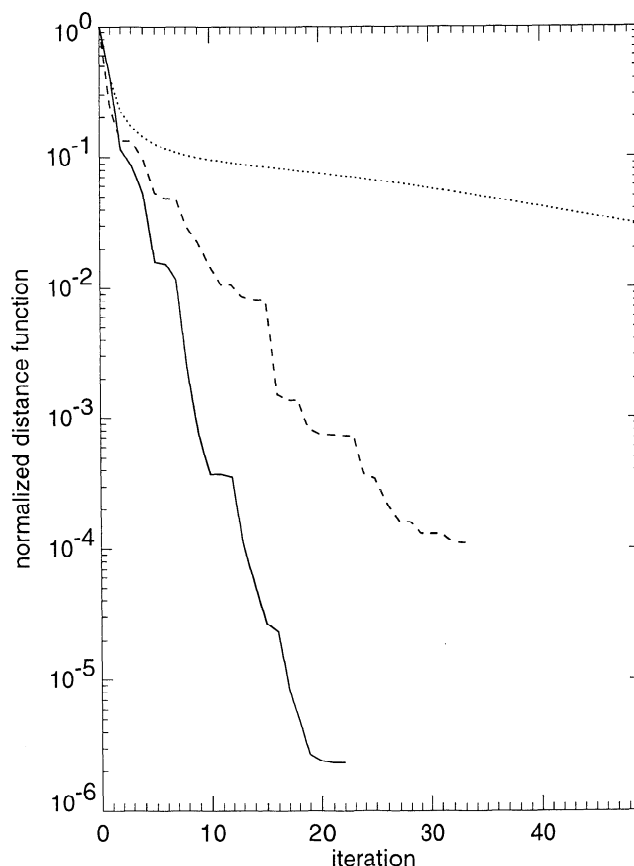


Figure 3. Minimization of the normalized distance function as function of number of iterations by steepest descent method (dotted line), BFGS algorithm without preconditioning (dashed line), and BFGS with preconditioning (solid line).

After 23 iterations the model performance was accepted as sufficiently close to the “observations” which is indicated by the distance function ceasing to decrease below a preselected threshold value during the iteration. Figure 3 shows the distance function as a function of the number of iterations, where the performances of three different methods are given: a simple steepest-descent method, BFGS-algorithm without preconditioning in the distance function, and BFGS-algorithm with preconditioning. It is observed that the costs of the function and gradient evaluation of the model, which is the forward and backward integration, takes more than 99% CPU time of the entire minimization process for all minimization algorithms used. Therefore it is admissible to infer the differences in computational requirements of the different minimization methods for a single iteration step from Figure 3. The superiority of the BFGS method with preconditioning is clearly visible by a decrease of 6 orders of magnitude of the distance function, as compared to 4 and 1 order of magnitude without preconditioning and steepest-gradient method, respectively. Three items call for a closer examination, which will be given in the sequel: (1) the length of the assimilation interval, (2) the influence of the first guess on the assimilation performance, and (3) the ambiguities of VOC analyses by ozone measurements.

4.3. On the Length and Position of the Assimilation Interval

For a thorough analysis of a case study it may be convenient to span the assimilation interval over the entire length of available measurements. However, in practice with spatial extensions of the model dimension, the computational expenditure will only admit of a time window of some hours. Since the most prominent feature of the variational approach is its ability to exploit the information inherent in the temporal variation of measured constituents, it is expedient to include the dawn or dusk hours to analyze photolysis-dominated

gas phase chemistry. The chemical mechanism then exhibits a high variance on a comparably short timescale with reduced computational demands.

Figure 4 displays the differences in assimilation skill for ozone of the identical twin experiment, when ending the assimilation interval already after 3 hours at 0600 LT, as compared to 5 hours alluded to earlier. Both runs have the first guess and the starting time of 0300 LT in common, which is depicted by the thin solid line. The reference run to be approximated is given by the long-dashed line. The performance of the assimilation run with 3 hours is shown by the short-dashed line, which differs considerably from the reference run. This result can be readily explained by comparison of the first guess run with observation run, where significant differences do not occur before 0600 LT and no distinct information is available for the assimilation algorithm. The ozone values as inferred from the full 5-hour assimilation interval are repeated for comparison by a bold line.

4.4. Impact of the First Guess Quality on the Assimilation Skill

An important question is which deviation from “truth” must not be exceeded by the first guess values to result in a successful assimilation? This problem is intimately related to the question to which extent the final analyses are uniquely determined or dependent on the choice of the first guess.

To this end eight additional identical twin experiments were carried out, where only the first guess values of the constituents were modified, as summarized in Table 1.

Two extreme cases are included here by (1) setting all values to 0.1 ppbv (experiment VIII), and (2) by increasing all values by 1 order of magnitude compared to the observation run (experiment IX). The stop condition is defined by a small threshold value $\Delta\mathcal{J} = (\mathcal{J}(\mathbf{x}^n) - \mathcal{J}(\mathbf{x}^{n+1}))/\mathcal{J}(\mathbf{x}^0) = 10^{-3}$, indicating

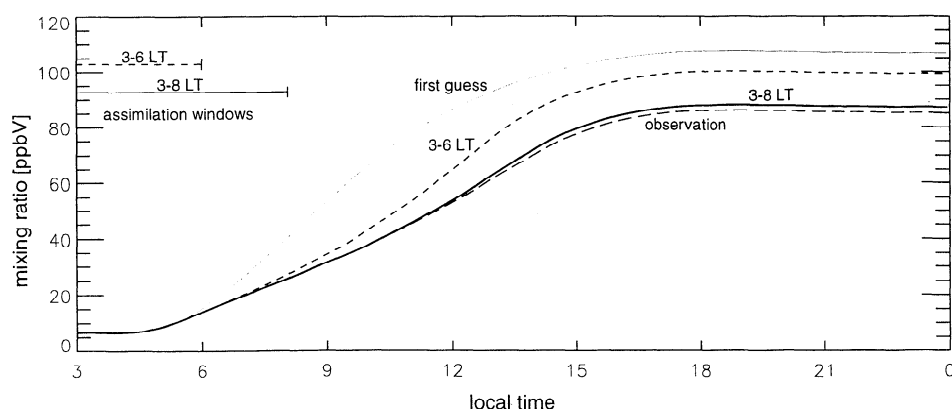


Figure 4. Performance of assimilation skill with time window from 0300 to 0600 LT (short-dashed line), and from 0300 to 0800 LT (bold solid line). First guess run (thin solid line) and “observation” run (long-dashed line) are given for reference.

Table 1. Impact of the First Guess Quality on the Convergence Rate

Experiment	Characterization of the First Guess ^a	$J(\text{First Guess})$
I	$\mathbf{X}^I(t_0) = 0.8 \mathbf{X}^0(t_0)$	0.11
II	$\mathbf{X}^{II}(t_0) = 1.2 \mathbf{X}^0(t_0)$	0.15
III	$\mathbf{X}_i^{III}(t_0) = 0.5 \mathbf{X}_i^0(t_0)$ for species with odd index i and $\mathbf{X}_i^{III}(t_0) = 2.0 \mathbf{X}_i^0(t_0)$ for even i	0.21
IV	$\mathbf{X}^{IV}(t_0) = 0.5 \mathbf{X}^0(t_0)$	1.00
V	$\mathbf{X}_i^V(t_0) \in \{400, 5, 0.5, 0.01, 0.001 \text{ ppbv}\}$ (see section 4.2)	1.70
VI	$\mathbf{X}^{VI}(t_0) = 2.0 \mathbf{X}^0(t_0)$	2.68
VII	$\mathbf{X}^{VII}(t_0) = 0.1 \mathbf{X}^0(t_0)$	3.55
VIII	$\mathbf{X}^{VIII}(t_0) = 0.1 \text{ ppbv } \forall i$	4.45
IX	$\mathbf{X}^{IX}(t_0) = 10.0 \mathbf{X}^0(t_0)$	67.45

^a $\mathbf{X}^0(t_0)$ represents the initial concentration of the “observation” or reference run.

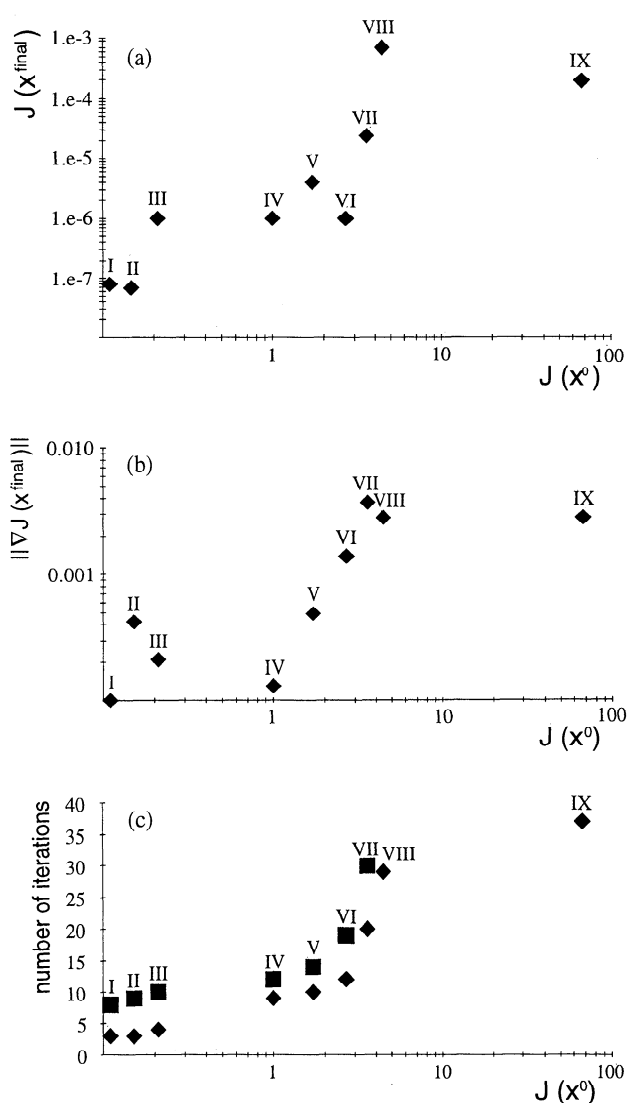


Figure 5. Impact of the first guess' quality on the convergence rate: (a) final value J^{final} of the distance function versus first guess' value $J(\mathbf{x}^0)$, (b) $\|\nabla_{\mathbf{x}(t_0)} J\|$ versus $J(\mathbf{x}^0)$, and (c) number of iteration steps to reduce the distance function by $\epsilon = 1.0 \times 10^{-3}$ (diamond) and $\epsilon = 1.0 \times 10^{-4}$ (square).

the minimal stepwise reduction of the distance function.

The results are presented in Figure 5a by a logarithmic scatterplot, where the final value of the distance function versus the initial value is given for each experiment. Figures 5b and 5c alternatively present the norm of the distance function's final gradient and the number of iterations required to reduce the distance function below the arbitrarily chosen absolute threshold values 10^{-3} and 10^{-4} , respectively. All displays clearly indicate that the smaller the initial distance function the more favorable is the assimilation result in terms of both smallness of the distance function and low number of iterations. However, additional iterations of poor first guess runs lead to further reductions of the distance function and a closer match with observations for those species which have been shown to be analyzed favorably in a previous subsection. It can be concluded that insufficient preconditioning of the minimization algorithm hampers further progress in minimizing the distance function.

Since the gas kinetic equations are highly nonlinear, it is still not guaranteed that no secondary minimum is approximated by the minimization procedure. Nevertheless, no evidence is found that there is another minimum which may have attracted the state variables, even when starting far off the “true” minimum. This is in accord with the experience in meteorological applications by Talagrand [1991], who has not encountered problems with ambiguous minima.

4.5. Analysis of VOC-Concentrations by Ozone Measurements

Although the VOCs are, together with NO_x , the most important constituents for anthropogenic ozone production, the assimilation process does not succeed to reproduce their individual initial values. The only exception from this is formaldehyde and, with lesser skill, higher aldehydes. A possible means to characterize the total VOC contents is given by their total concentration in terms of ppbc (where the ppbv value of the various

Table 2. Analysis of Total Carbon Concentration for Different First Guesses and Relative Approximation to the True Value Which is 49.5 ppbC

Experiment	VOC Initial Concentration		Error Reduction, %
	First Guess	Final Result	
I	39.6	44.4	48.5
II	59.4	54.4	50.5
IV	24.7	36.1	46.0
VI	99.0	77.6	43.2
VII	5.0	18.3	29.9
IX	495.0	278.0	48.7

Total carbon concentration in ppbC.

hydrocarbons is multiplied by their number of carbon atoms).

Table 2 summarizes the limited feasibility of the assimilation procedure to determine the ppbc concentrations for some of the experiments described above. It can be seen from the error reduction column that there is only a significant tendency to analyze the ppbc concentrations toward the “true” ppbc levels of the observation run, with an approximation limited by about 40%. It is therefore not possible to analyze the ppbc concentrations without individual observations of VOCs.

However, the overall ozone creation potential of the ensemble of VOCs should be analyzed significantly better, since otherwise the satisfying reproduction of the ozone curve would have failed. It must be concluded

that the VOCs can substitute each other to a sufficiently large extent to achieve the observed ozone values. With the available observations in the present case, matrix \mathcal{R} in (17) is suspected to be close to singularity.

4.6. Influence of Measurement Errors

The problem is considered where measurements have errors which are assumed to be unbiased and uncorrelated both in time and with respect to other species. Conditions are as in the identical twin experiment of subsection 4.2 except that “measured” time series of O_3 and NO_2 are provided to the assimilation algorithm ($g = 2$ and $N = 60$) which are artificially corrupted by random errors. The error distribution is defined to be Gaussian, which also means unbiased, with a variance of 5% of the species’ concentration.

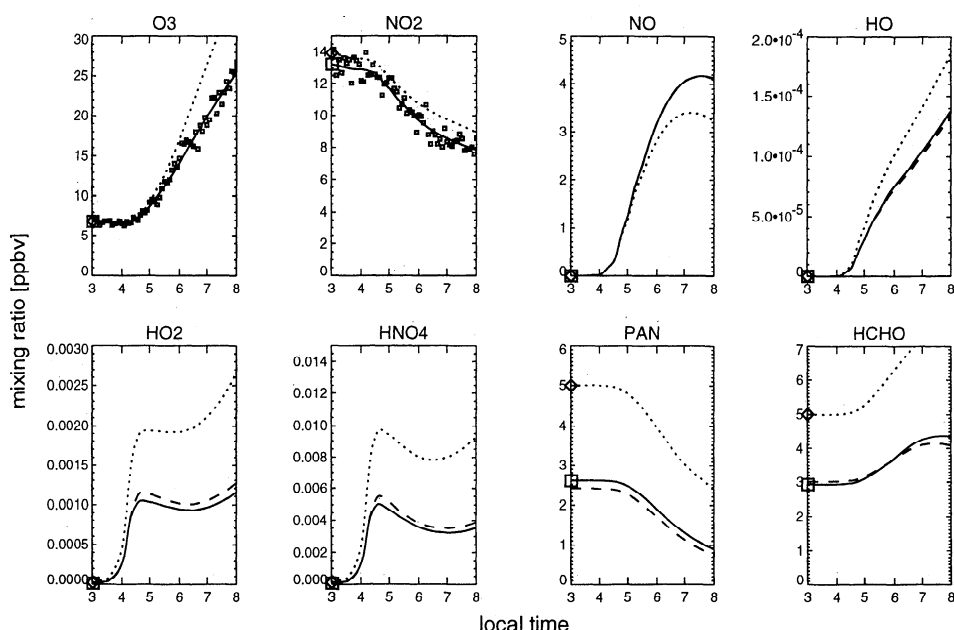


Figure 6. Performance of assimilation skill with “observations,” to which artificially unbiased Gaussian errors are superimposed by random generation (open squares). Variances of the “observation errors” are defined to be 5% of the actual concentration. Plotting conventions as in Figures 1 and 2.

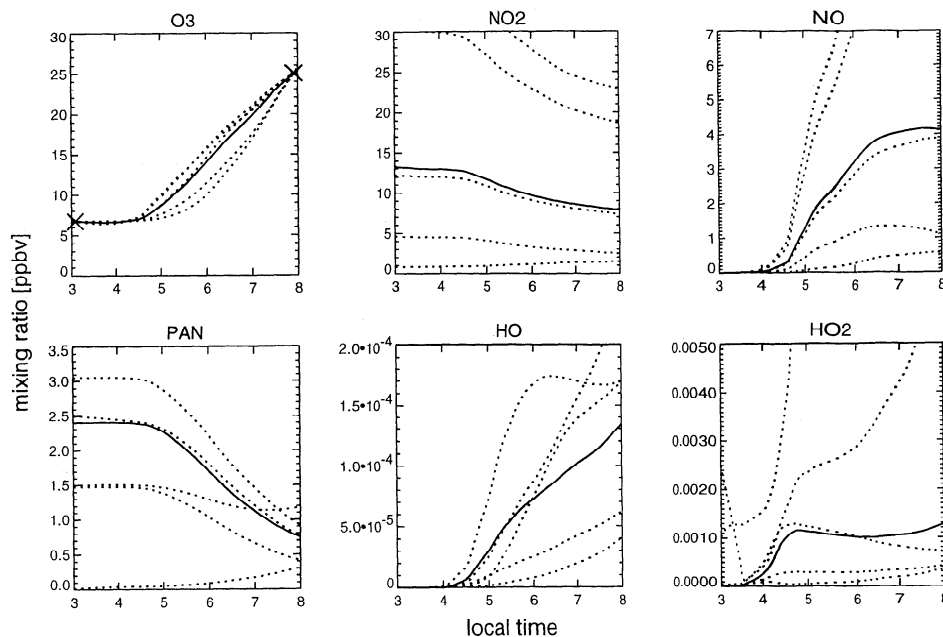


Figure 7. Variance of analyses for six species, where only two “observations” of ozone were made available at the beginning and the end of the assimilation window, respectively (crosses). Solid lines denote the “observation” run, for reference. Dotted lines indicate assimilation results with different initial values.

Figure 6 demonstrates that the variational algorithm succeeds to assimilate the data as favorably as in the case of perfect measurements. It is evident that there must be sufficient “observations”, such that the unbiased character of the measurement error distribution is statistically significant.

Now no deterministic model trajectory in the phase space can perfectly fit the “observations” with their stochastically generated superimposed “errors”. Hence it is obvious that the distance function cannot be minimized to an arbitrarily small value. As in the case of error free “observations” a decrease of 1 order of magnitude is attained after six iterations but further minimization progress fades away.

4.7. Assimilation of Intermittent Data

In preparation of the next section two cases are now studied where “measurements” are available only at the beginning and at the end of the assimilation window. The first case considers ozone only data with the two “observations” available at 0300 and 0800 LT ($g = 1$ and $N = 2$).

A suite of simulations was performed, which differ only in terms of the the initial values chosen. The result is presented in Figure 7 for species, which have been shown above to be well analyzable when quasi-continuous “observations” were introduced. Although in all cases the two ozone measurements are fully approximated, it can be seen that intermediate concentration values may differ up to 50%. For all other species the degree of freedom left by only two ozone measurements is too high to claim any success for the analyses.

Only simulations for which the initial concentrations are selected close to the “true” values have resemblance to the observation run.

Results improve moderately if an additional pair of NO_2 measurement is made available as demonstrated in Figure 8. The ozone variations between the observation dates are limited by about $\pm 10\%$ as it is for NO, where no measurements were available. NO_2 appears to be rather precisely analyzed, whereas the analysis of other species fails. It must be concluded that two measurements of two species cannot give an acceptable analysis.

4.8. Sensitivity of the Analysis to Isolated Measurements

A Lagrangian multiplier $\lambda(t)$ can be interpreted as a sensitivity parameter with respect to a perturbation $\delta \mathbf{x}(t)$ of a state function $\mathbf{x}(t)$, to which $\lambda(t)$ is the adjoint variable. Zou *et al.* [1993b] describe a meteorological application of the adjoint method for sensitivity studies.

An alternative and more basic algorithm is presented by Fisher and Lary [1995], which is adopted in this study. Given an isolated observation increment or small perturbation $\Delta x_j(t_n)$ of species j at time t_n , integration of (11) backwards in time from t_n to t_m then provides Lagrangian multipliers as sensitivity parameters $\lambda_i(t_m)$, at earlier instants $t_m < t_n$, with respect to $\lambda_j(t_n) = \Delta x_j(t_n) = \partial J / \partial x_j(t_n)$.

Due to the linearity of the operators in (11), a perturbation of a single species k at time t_l contributes to the distance function J by

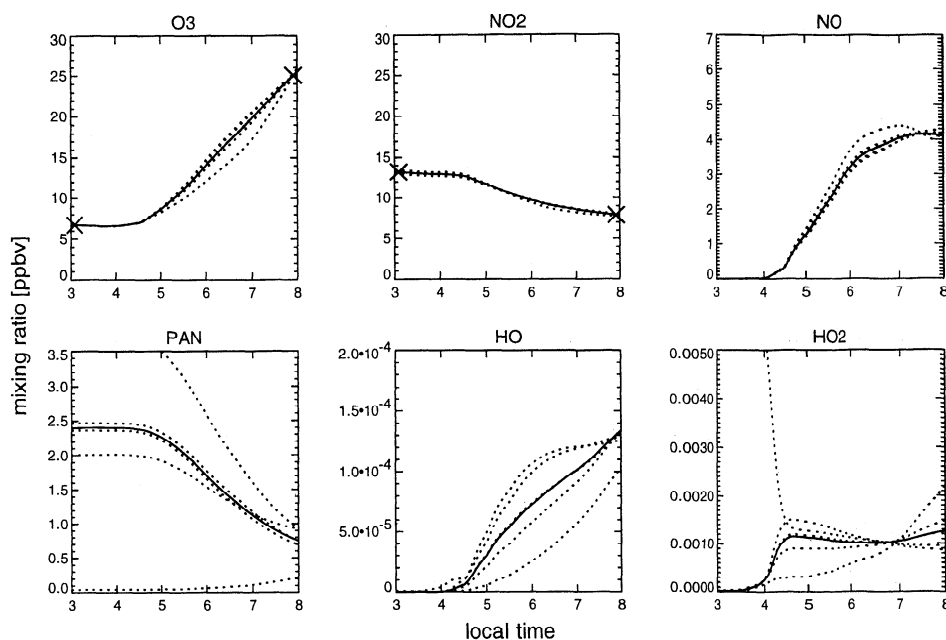


Figure 8. Variances of analyses as in Figure 7, but two additional NO₂ “observations” were made available to the algorithm.

$$\delta \mathcal{J} = x_k(t_l) \frac{\partial \mathcal{J}}{\partial x_k(t_l)} \frac{\delta x_k(t_l)}{x_k(t_l)}. \quad (19)$$

Here the expression is divided for expansion by the concentration $x_k(t_l)$ to obtain the sensitivity with respect to a normalized perturbation.

Based on these considerations, *Fisher and Lary* [1995] proposed an “influence function” $\gamma_{ij}(t_m, t_n)$ which gives the relative contribution of species i at time t_m to adjust a single species j to an observation at time t_n ,

$$\gamma_{ij}(t_m, t_n) = \frac{x_i(t_m)}{x_j(t_n)} \frac{\frac{\partial \mathcal{J}}{\partial x_i(t_m)}}{\Delta x_j(t_n)}. \quad (20)$$

The use of the influence function can be helpful in different ways. Two applications may serve as an illustration. The question is addressed which trace species should be measured to gain maximal benefit for the assimilation. We restrict our focus on three measurements of hydrocarbons and, mainly for expository purposes, on CO. Figure 9 displays the influence functions of species $j \in \{\text{CO}, \text{HC3}, \text{HC8}, \text{XYL}\}$ with respect to the five most important species i , due to forcing of the species j at time $t_n = 0800$ LT (for the definition of the RADM2 groups see *Stockwell et al.* [1990]). In the case of CO it can be clearly seen from Figure 9a, that a perturbation at the final time t_n can be effectuated nearly exclusively by CO alone with the like perturbation at earlier times $t_m < t_n$. The impact on other species, of which the graphs of the four strongest are included in each panel, are very close to the zero line and obviously negligible. Under chemical conditions determined by the preselected initial concentrations, the assimilation interval, meteorological, and radiative conditions, it can therefore be concluded that the benefit of CO measure-

ments is small since there is no information conveyed about other unobserved species.

In the case of the hydrocarbons the influences of the “measurements” of HC3, HC8, and XYL on other species are qualitatively similar to each other but differ quantitatively by about 1 order of magnitude, as visible from Figure 9b–d, respectively. More specifically, NO₂ and ozone are positively affected, while PAN and formaldehyde are the most negatively affected species on a timescale of 5 hours, embracing dawn with clear sky conditions. The differences in relative magnitudes reflect the reactivity of the reference species with OH, where the reaction rates read for HC3: $3.2 \times 10^{-1} \text{ ppm}^{-1} \text{ s}^{-1}$; HC8: $2.5 \times 10^{-2} \text{ ppm}^{-1} \text{ s}^{-1}$; and XYL: $6.9 \times 10^{-2} \text{ ppm}^{-1} \text{ s}^{-1}$. Hence, the measurement of xylene is most promising among the considered VOCs to analyze other species like NO_x, O₃, and PAN.

The interaction of NO, NO₂, and O₃ in terms of the influence function is already discussed by *Fisher and Lary* [1995] for stratospheric conditions on the basis of a 36 hours assimilation interval. In fact, the observation of any one of these species contains a large amount of information about the other two constituents. Figure 10 displays the influence functions of O₃, NO, and NO₂ for lower tropospheric conditions and 5 hours assimilation windows, centered around both dawn and dusk. As a consequence of photochemical breakdown, it is indicated in Figure 10a that daytime observations (0800 LT) of NO get lost for analyses of NO during nighttime but the information is conserved in NO₂ and, to a much lesser extent, in ozone. Nighttime measurements (2200 LT) of NO can formally be used as well, as can be seen from Figure 10b, but are of minor value in practice due to the very small concentrations observed. Daytime ozone observations can give information about

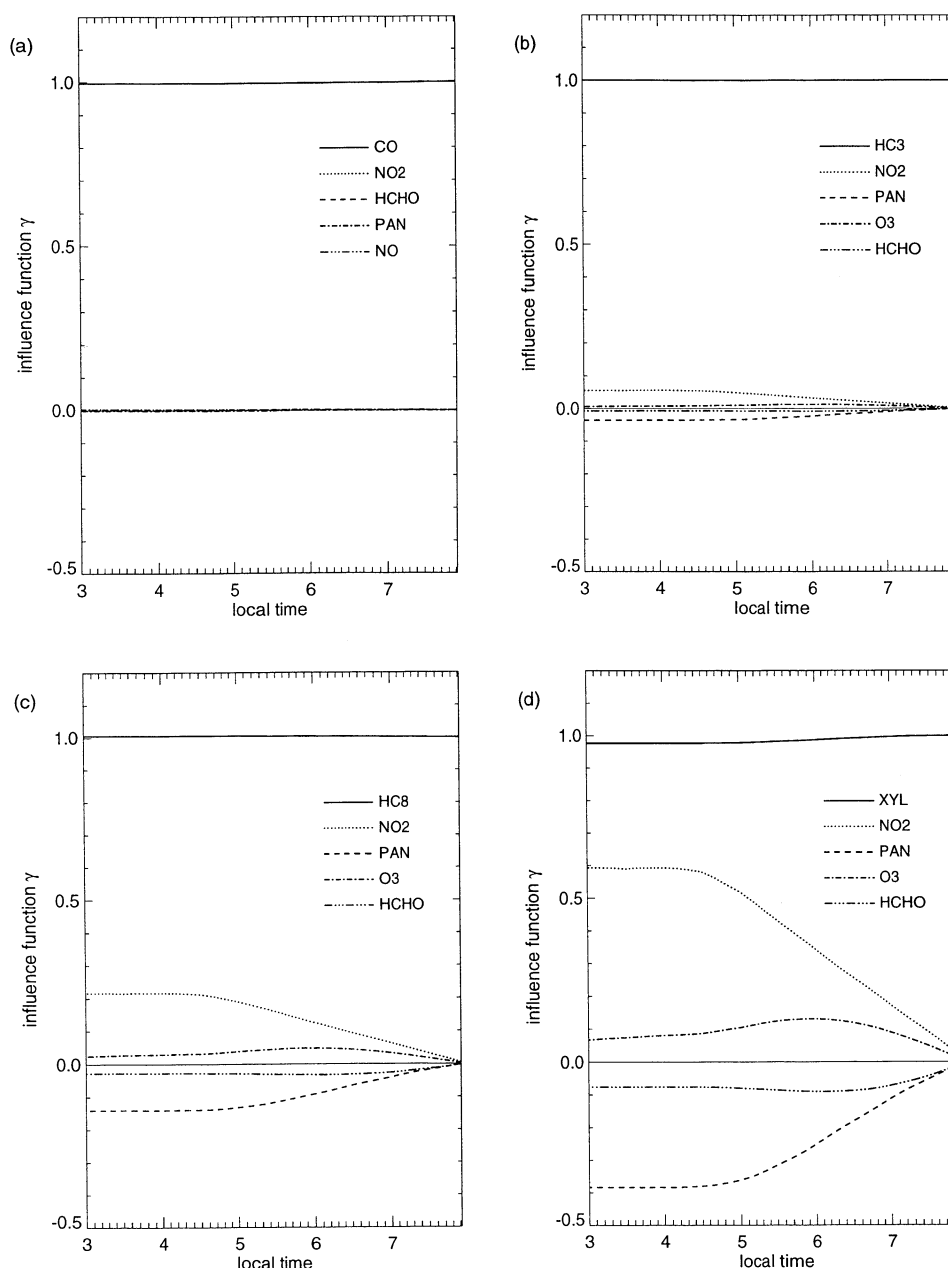


Figure 9. Graphs of the influence functions due to an isolated perturbation at the end of the assimilation interval well after sunrise (0800 LT) for (a) CO, (b) HC3, (c) HC8, and (d) XYL. The graphs of the four most impacted species other than the perturbed species are included.

nighttime PAN and NO₂ levels; however, it is of reduced importance with respect to ozone itself before sunrise. On the other hand, evening measurements of ozone contain information on NO, NO₂, and ozone itself before sunset, but not for PAN (not shown in Figure 10d). Finally, NO₂ morning observations give only reduced information on ozone, while for an evening observation the reverse is true.

The results of this subsection can merely show a first-order link of cause and effect by the variational assimilation method, since only a single “observation” is introduced. Again it should be pointed out that full time series, unlike single observations considered here, con-

vey much more information which then can be exploited for the analysis of many other species not necessarily appearing to be sensitive in terms of the influence function.

5. A Real Data Experiment

5.1. Local Orography, Available Data, and Meteorological Conditions

Although intended for use in an Eulerian model system, the availability of a comprehensive set of different measured species was an incentive to evaluate the adjoint RADM2 mechanism within the framework of a

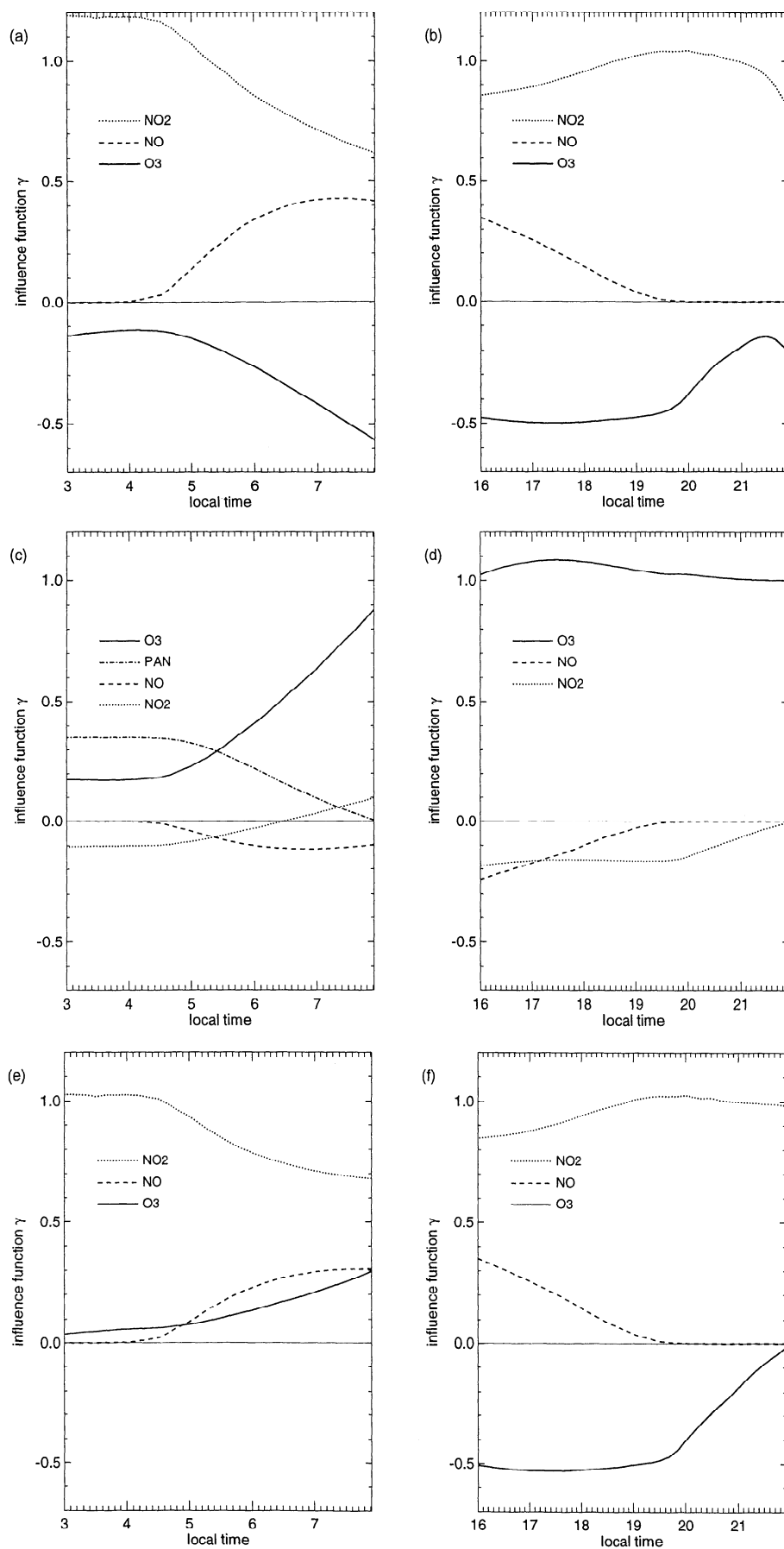


Figure 10. Influence functions as for Figure 9 (left panels), but additionally including an assimilation interval spanning sunset, ending at 2200 LT (right panels). Perturbed species are NO (a, b), O₃ (c, d), and NO₂ (e, f).

Table 3. Total of Species Measured at Stations Schauinsland, Kappel, Appertaining RADM2 Group, and Indication on Usage in the Assimilation Algorithm

Species	RADM2 Group ^a	Kappel	Schauinsland	Assimilated
n-Butane	HC3		x	x
i-Pentane	HC5		x	x
n-Pentane	HC5		x	x
3-Methylpentane	HC5		x	x
2-Methylpentane	HC5	x	x	x
n-Hexane	HC5	x	x	x
i-Octane	HC5	x	x	x
2,4-Dimethylpentane	HC8	x	x	x
3-Methylhexane	HC8	x	x	x
n-Heptane	HC8	x	x	x
Methylcyclohexane	HC8	x	x	x
n-Octane	HC8	x	x	x
Hexene1	OLT		x	
Benzene	TOL		x	x
Ethylbenzene	TOL	x	x	x
Toluene	TOL	x	x	x
m/p-Xylene	XYL	x	x	x
o-Xylene	XYL	x	x	x
Isoprene	ISO	x	x	
O ₃	O3	x	x	x
NO	NO	x	x	x
NO ₂	NO2	x	x	x
NO _y	NO3, HNO3, ...	x	x	
PAN	PAN		x	x
CO	CO		x	x

^aFor the definition of the RADM2 groups see *Stockwell et al.* [1990].

Lagrangian approach. An observation station for numerous measurements of trace species was established on the Schauinsland mountain (47°54' N, 7°48' E, 1220 m above sea level (asl)) in the southern Black Forest, Germany, by the research centre Jülich.

Starting beneath the Schauinsland summit the “Gros-ses Tal” valley opens northward, where the suburb Kappel of the city of Freiburg is situated at its entrance 350 m asl. During a special observation period in September 1992, a second measurement station was mounted near the suburb but sufficiently apart from direct urban or traffic emission sources. The distance between the two stations is about 8.5 km.

Table 3 summarizes the two sets of measurements obtained from these stations. Observations were realized every half an hour, the errors of which were estimated to lie between 8% and 30% in the case of VOCs. Further to this, several meteorological parameters were observed like temperature, pressure, relative humidity, wind direction, wind speed, and photolysis rates for NO₂. A comprehensive description of the measurement sites is given, for example, by *Kramp et al.* [1995] and *Kramp and Volz-Thomas* [1997].

From long-term observations, it is known that during the occurrence of persistent northwesterlies the urban plume of Freiburg is channelled by the valley. The air masses are then forced to pass the Kappel and later

Schauinsland observation station. During the special observation period from September 15 to September 23, 1992, this was the case on September 17 starting shortly before noon.

5.2. Mapping of Campaign Observations on RADM2 Model Parameters

Modeling the physical and chemical states between Kappel and Schauinsland stations by a Lagrangian approach requires the estimation or inference of some meteorological and other parameters. In the present study these were estimated as follows:

1. Clear sky photolysis rates computed with the radiative transfer model of *Madronich* [1987] could be applied since there was no cloud cover. NO₂ photolysis rates observed at both stations are in good agreement with the computed values.

2. Temperature and relative humidity were available at both stations. Values at intermediate locations were linearly interpolated during the drift of the air parcel. Following *Kramp et al.* [1995] and *Kramp and Volz-Thomas* [1997], a diffusion rate of $(6.8 \pm 0.9) \times 10^{-5} \text{ s}^{-1}$ was inferred by budget calculations and taken here as first guess. Further, in those studies a drifting time of 154 min between Kappel and Schauinsland was estimated. Since pressure records were only available at Schauinsland, the hydrostatic equation was applied to

Table 4. Fraction of Observed VOC Species at Kappel and Schauinsland Station Relative to the Tauern Road Tunnel Experiments by *Gregori et al.* [1989]

RADM2 Group ^a	Observed Fraction of the Group, %	
	Kappel	Schauinsland
HC3	–	26.5
HC5	27.6	93.8
HC8	27.7	27.7
OLT	–	unknown
TOL	70.1	96.3
XYL	60.0	60.0

^aFor the definition of the RADM2 groups see *Stockwell et al.* [1990].

extrapolate the pressure at the Kappel station and at intermediate locations.

3. Dry deposition rates are inferred as described by *Chang et al.* [1987], while the mixing height was adjusted to vary the dry deposition. The mixed forest classification for land use was taken.

4. There are no anthropogenic emission sources along the pathway of the air parcel. Isoprene concentrations measured at both stations are sufficiently low to neglect emission rates.

Since observed VOCs do not comply with the RADM2 VOC classification, further assumptions must be invoked for the pertinent mapping from measurements to the lumped species of the model. Comparing the ratios of the measured VOCs, *Kramp et al.*

[1995] found them in close agreement with measurements made in the Tauern road tunnel by *Gregori et al.* [1989] which show pure car traffic characteristics. The Tauern tunnel measurements are reported to comprise 90% of the total carbon contents and may then well serve as a key for mapping the Schauinsland and Kappel measurement on RADM2 categories. The resulting correspondences are given in Table 4 which summarizes the percentages of measured concentrations in ppbc relative to RADM2 categories. With this mapping we therefore have now $N = 2$, $g(\text{Kappel}) = 7$, and $g(\text{Schauinsland}) = 10$.

5.3. Assimilation of Real Measurements

As a base case version the first assimilation run was started 5 min before 1237 LT with the Kappel observation and ended at 1511 LT at Schauinsland after 154 min integration time, where the unsynchronized half hourly sampling time intervals of the gas chromatographs stipulated a maximal inaccuracy of 30 min. Initial values taken as first guess in the Schauinsland case were either the observed values at Kappel, if actually measured, or standard values for an urban plume scenario. The 5 min starting time prior to the Kappel date was selected to allow for relaxation of the chemistry mechanism, since the minimization routine does not necessarily keep the chemical composition linked with a more natural state close to equilibrium. This is an analogon to the initialization problem encountered in meteorological data assimilation. The detrimental effect is by far less critical here, since gas kinetics are

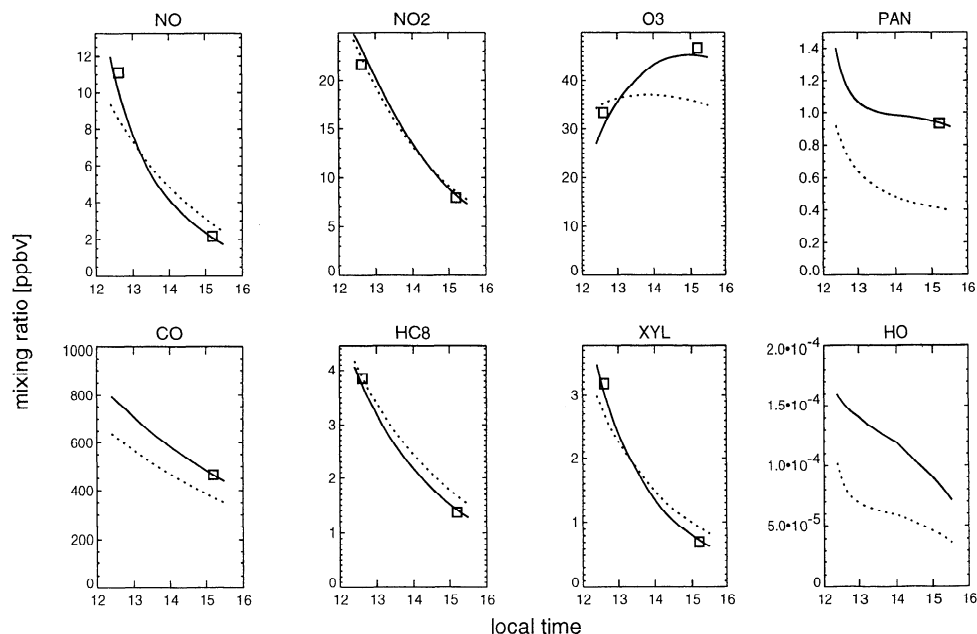


Figure 11. Assimilation results for the measurement stations Kappel (squares at 1237 LT observation time) and Schauinsland (squares at 1511 LT) shown by solid lines. First guess run is depicted by dotted lines. Simulation experiment with optimized parameters for vertical mixing, dry deposition, and drifting time between the stations is given.

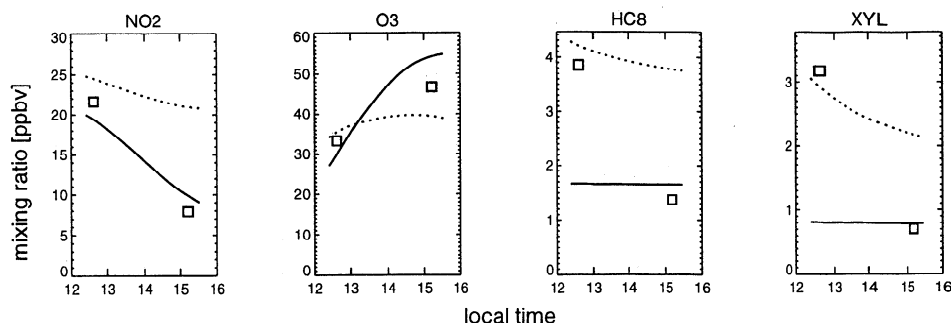


Figure 12. Assimilation results without diffusion and deposition. Plotting conventions as for Figure 11.

expressed by a first-order differential equation system. The final assimilation result proved to be quite insensitive to the choice of the first guess.

Figure 11 displays the assimilation result for five species observed at both locations, for CO and PAN, which are only measured at Schauinsland, and HO without observations. Considerable improvements can be ascertained for the formation of ozone as key species. Taking the distance function as a quality criterion for as yet undefined simulation parameters, the diffusion constant was varied by finite steps to minimize the value of J . It turned out that the diffusion rate as inferred by our approach is close to the upper error margin of the value found by Kramp *et al.* [1995]. A remarkably good result was then obtained for example for PAN, where the analysis algorithm led to a doubling of the concentration to fit the measured value exactly.

The role of the diffusion is appreciable when setting its coefficient to 0. The result for four species is given in Figure 12, where the missing reduction of NO₂ and O₃ by vertical transport aloft is clearly visible. This is the more the case for species where the background values outside the urban plume are small as demonstrated for XYL. Without diffusion the model is utterly incapable to simulate the observed decrease by chemical destruction alone.

6. Summary and Discussion

The feasibility to assimilate observations which are arbitrarily distributed over a time span is often quoted to be the prime advantage of variational adjoint analysis methods. However, it is demonstrated that even a poorly resolved time series can comprise much useful information such that it is possible to benefit from the knowledge of the gas kinetic system as it is condensed in advanced models. In recompense, the significant advantages of the method to give a consistent interpretation of observations is therefore limited by the model skill.

It is shown that with a sufficiently well resolved time series of only one species, it is possible to analyze other unmeasured species. While in our experiments focusing on ozone measurements the NO_x concentrations are determined quite exactly, VOCs are analyzed only in the

limits to effectuate the proper simulation of the measurements. The smaller the time window the relatively larger is the validity of the tangent linear approximation and consequently the larger is the possibility of the VOCs to substitute each other in their effect to reproduce ozone observations, as demonstrated in subsection 2.4. In cases like this it is often possible to introduce external knowledge like the relative concentrations of VOCs to the assimilation scheme defining the background term as included in (1). However, the knowledge of origin and quality of pollutive burden, as, for example, obtained from traffic tunnel campaigns, should be sufficiently exact. The assimilation algorithm can then be modified to maintain the presumed relative VOC split. In general, any knowledge about interdependencies of measured and unmeasured species can be exploited by use in the background term of the distance function. To this end the error margins of that knowledge have to be estimated to define the diagonal and off-diagonal elements of the background error covariance matrix. This procedure may finally prevent that, although consistent with provided measurements, the assimilation procedure possibly leads to a drift of not measured species to evidently unreasonable initial values.

By means of the adjoint mechanism it is further possible to assess the relative benefit of observations of individual species to the analysis. As it was demonstrated by xylene in subsection 4.8, a significant change of concentration within the time span of the assimilation window gives a promising prospect for a favorable assimilation. This question is closely related to the application of the influence function which gives direct evidence of the relative extent of interactions between different constituents.

The adjoint approach may also exhibit model deficiencies or systematic biases, provided observations are sufficiently complete and accurate and the error of representativeness is negligible. It should then be feasible to minimize the sources of possible model errors such as inaccurate emission rates, insufficient parameterization of exchange processes with elevated layers, and poorly known deposition rates.

Comparing the present study with the different focus of *Fisher and Lary* [1995] three more specific items are worth mentioning:

1. The length of assimilation window can be reduced to some hours, provided changes in the photolysis rates force the gas kinetic mechanism to execute highly variable concentration changes. In this case a tangent linear approximation to the evolution of the state variable would rapidly lose validity and the nonlinear chemical interactions of many important constituents offer prospects to analyze unobserved data or at least to reduce the manifold of initial states consistent with later observations.

2. A further item is the question on the usefulness to take comprehensive gas phase mechanisms like RADM2 for assimilation while only a small fraction of constituents or only one is measured. However, if model runs with roughly determined initial values, like seasonal averages, give useful results, this is more the case for model output based on more carefully determined initial values. In the latter case either the predictive skill of the model is improved or the model deficiencies can easier be identified.

3. As demonstrated in the 'Schauinsland' real data assimilation, a major source of errors can be identified in insufficiently known dynamics and other parameters describing the state of the local atmosphere, namely vertical exchange rates and the deposition rate. In this study the effect described by these parameters to dilute the urban plume is estimated via finite variations which lead to a satisfactory result in the present case. However, assimilation of meteorological data by an adequate, say, a 4D-var meteorological assimilation scheme is clearly desirable.

The conclusion is that not only in the stratosphere, where satellite data are available, but also in the planetary boundary layer with few observations, variational adjoint data assimilation can be successfully applied for a comprehensive gas phase mechanism.

The weak points which became evident in the Schauinsland data assimilation, also admit for solution by a variational approach. This is not only true for the meteorological parameters by a 4D-var method of a regional meteorological driver model. Rather, emission and deposition rates, or vertical exchange coefficients, may be estimated by an adjoint model as well.

Since the above experience indicates the necessity of three-dimensional meteorological modeling, the adjoint of the gas phase mechanism is a first step toward a full 4D-var assimilation scheme, based on an Eulerian approach. This concept requires the inclusion of the adjoint advection and diffusion operators, and, in a mature phase, also adjoint cloud parameterizations. In this case estimations of effects other than gas phase conversion are less speculative as in the Schauinsland case. The gain in predictive skill can be more confidently assessed and the identification of systematic model biases will then be less difficult.

Nevertheless, it must be noted that the computational requirements increase rapidly with further dimensional extensions. CPU time of an adjoint code is about twice as high as for the corresponding forward code and numerous iterations are often required. Uncertainties in the suitable background concentrations of other height levels than the lowest one and missing in situ observations at elevated levels make satellite data as expected from advanced global ozone monitoring experiment (GOME) [*Chance and Burrows*, 1993] retrieval algorithms indispensable.

A concurrent approach which is also feasible for chemistry data assimilation is Kalman filtering. While computational demands are considerably higher, the practicability to account for model deficiencies during the assimilation process is a significant advantage of this method, provided both model proclivities and unbiased errors of the model are sufficiently well known. As stated above, this is not the case on a safe statistical basis since high-quality analyses of the chemical state of extended surface areas are not yet available for comparison. Therefore the variational approach applied in this study appears to be the more practical one if spatial or dimensional extensions are intended.

Acknowledgments. Special thanks are due to D. Kley and H. Geiss, Research Center Jülich (F.R.G.), who gave us access to the Schauinsland data set. The authors are greatly indebted for fruitful discussions with O. Talagrand, ENS Paris, J. Chang, SUNY, Albany (N.Y.), W. Stockwell, IfU Garmisch-Partenkirchen (F.R.G.), and H. Geiss. Financial support was provided by the European Union's Climate and Environmental program under grant ENV4-CT95-0024, the Troposphärenforschungsschwerpunkt of the German Ministry for Education, Science, Research, and Technology (BMBF) under grant 07TFS 10/LT1-C.1, and the Ministry for Science and Research (MWF) of Northrhine-Westfalia. Computational support was provided by the Central Institute for Applied Mathematics (ZAM) of the Research Center Jülich and the Regional Computing Center (RRZK) of the University of Cologne.

References

- Altshuller, A. P., Measurements of the products of atmospheric photochemical reactions in laboratory studies and in ambient air - relationships between ozone and other products, *Atmos. Environ.*, 17, 2383-2427, 1983.
- Austin, J., Toward the four-dimensional assimilation of stratospheric chemical constituents, *J. Geophys. Res.*, 97, 2569-2588, 1992.
- Bennett, A., *Inverse Methods in Physical Oceanography*, 346 pp., Cambridge Univ. Press, New York, 1992.
- Bertsekas, D. P., *Constrained Optimization and Lagrange Multiplier Methods*, 410 pp., Academic, San Diego, Calif., 1982.
- Byrd, R., P. Lu, J. Nocedal, and C. Zhu, A limited memory algorithm for bound constrained optimization, *Tech. Rep. NAM-08*, 24 pp., Northw. Univ., Evanston, Ill., 1994.
- Chance, K. V., and J. P. Burrows, SCIAMACHY and GOME: The scientific objectives, in *Optical Methods in Atmospheric Chemistry*, edited by H. J. Schiff and U. Platt, *Proc. SPIE Int. Soc. Opt. Eng.*, 1715, pp. 502-512, 1993.

- Chang, J. S., R. A. Brost, I. S. A. Isaksen, S. Madronich, P. Middleton, W. R. Stockwell, and C. J. Walcek, A three-dimensional Eulerian acid deposition model: Physical concepts and formulation, *J. Geophys. Res.*, **92**, 14,618-14,700, 1987.
- Chao, W. C., and L.-P. Chang, Development of a four-dimensional variational analysis system using the adjoint method at GLA, 1, Dynamics, *Mon. Weather Rev.*, **120**, 1661-1673, 1992.
- Courtier, P., J.-N. Thépaut, and A. Hollingsworth, A strategy for operational implementation of 4D-Var, using an incremental approach, *Q. J. R. Meteorol. Soc.*, **120**, 1367-1387, 1994.
- Daley, R., *Atmospheric Data Analysis*, 457 pp., Cambridge Univ. Press, New York, 1991.
- Finlayson-Pitts, B. J., and J. N. Pitts, *Atmospheric Chemistry*, 1098 pp., Wiley-Interscience, New York, 1986.
- Fisher, M., and D. J. Lary, Lagrangian four-dimensional variational data assimilation of chemical species, *Q. J. R. Meteorol. Soc.*, **121**, 1681-1704, 1995.
- Gear, C. W., *Numerical Initial Value Problems in Ordinary Differential Equations*, Prentice-Hall, Englewood Cliffs, N. J., 1971.
- Gregori, M., C. Lanzerstorfer, H. Oberlinniger, H. Puxbaum, P. Biebl, O. Gläser, and J. Villiger, Tauerntunnel-Luftschadstoffuntersuchung 1988, *Rep. 4/89*, 109 pp., Abt. für Umweltanalytik, Inst. für Anal. Chem., TU Wien, Vienna, 1989.
- Hass, H., H. J. Jakobs, and M. Memmesheimer, Analysis of a regional model (EURAD) near surface gas concentration predictions using observations from networks, *Meteorol. Atmos. Phys.*, **57**, 173-200, 1995.
- Hov, Ø., Z. Zlatev, R. Berkowicz, A. Eliassen, and L. P. Prahms, Comparison of numerical techniques for use in air pollution models with nonlinear chemical reactions, *Atmos. Environ.*, **23**, 967-983, 1989.
- Kramp, F., and A. Volz-Thomas, On the budget of OH radicals and ozone in an urban plume from the decay of C5-C8 hydrocarbons and NOX, *J. Atmos. Chem.*, in press, 1997.
- Kramp, F., D. Kley, and A. Volz-Thomas, Die Rolle reaktiver Kohlenwasserstoffe bei der Photooxidantienbildung in ländlichen Gebieten, *Ber. des Forsch. Jülich 3050*, 176 pp., Jülich, Germany, 1995.
- Le Dimet, F. X., and O. Talagrand, Variational algorithms for analysis and assimilation of meteorological observations: Theoretical aspects, *Tellus*, **38A**, 97-110, 1986.
- Lewis, J. M., and J. C. Derber, The use of adjoint equations to solve a variational adjustment problem with advective constraints, *Tellus*, **37A**, 309-322, 1985.
- Madronich, S., Photodissociation in the atmosphere, 1, Actinic flux and the effects of ground reflections and clouds, *J. Geophys. Res.*, **92**, 9740-9752, 1987.
- McRae, G. J., W. R. Goodin, and J. H. Seinfeld, Numerical solution of the atmospheric diffusion equation for chemically reacting flows, *J. Comput. Phys.*, **45**, 1-42, 1982.
- Navon, I. M., X. Zou, J. Derber, and J. Sela, Variational data assimilation with an adiabatic version of the NMC spectral model, *Mon. Weather Rev.*, **120**, 1433-1446, 1992.
- Parrish, D., and J. Derber, The national meteorological centre's spectral statistical-interpolation analysis system, *Mon. Weather Rev.*, **120**, 1747-1763, 1992.
- Salby, M. L., Sampling theory for synoptic satellite observations, I, Space time spectra, resolution, and aliasing, *J. Atmos. Sci.*, **39**, 2577-2600, 1982a.
- Salby, M. L., Sampling theory for synoptic satellite observations, II, Fast Fourier synoptic mapping, *J. Atmos. Sci.*, **39**, 2601-2614, 1982b.
- Sandu, A., F. A. Potra, G. R. Carmichael, and V. Damian, Efficient implementation of fully implicit methods for atmospheric chemical kinetics, *J. Comput. Phys.*, **129**, 101-110, 1996.
- Stockwell, W. R., P. Middleton, J. S. Chang, and X. Tang, The second-generation regional acid deposition model chemical mechanism for regional air quality modeling, *J. Geophys. Res.*, **95**, 16,343-16,367, 1990.
- Stockwell, W. R., A homogeneous gas phase mechanism for use in a regional acid deposition model, *Atmos. Environ.*, **20**, 1615-1632, 1986.
- Talagrand, O., The use of adjoint equations in numerical modeling of the atmospheric circulation, in *Proceedings of Workshop on Automatic Differentiation of Algorithms: Theory, Implementation and Application*, edited by A. Griewank and G. G. Corliss, Soc. for Ind. and Appl. Math., Philadelphia, Pa., 1991.
- Talagrand, O., and P. Courtier, Variational assimilation of meteorological observations with the adjoint vorticity equation, I, Theory, *Q. J. R. Meteorol. Soc.*, **113**, 1311-1328, 1987.
- Zou, X., I. M. Navon, M. Berger, K. H. Phua, T. Schlick, and F. X. Le Dimet, Numerical experience with limited-memory quasi-Newton and truncated Newton methods, *SIAM J. Control Optim.*, **3**, 582-608, 1993a.
- Zou, X., A. Barcilon, I. M. Navon, J. Whitaker, and D. J. Cacuci, An adjoint sensitivity study of blocking in a two-layer isentropic model, *Mon. Weather Rev.*, **121**, 2833-2857, 1993b.

A. Ebel, H. Elbern, and H. Schmidt, University of Cologne, Institute for Geophysics and Meteorology, Project EURAD, Aachener Str. 201-209, 50931 Köln, Germany. (e-mail: eb@eurad.uni-koeln.de, he@eurad.uni-koeln.de, hs@eurad.uni-koeln.de)

(Received January 18, 1997; revised April 17, 1997; accepted April 22, 1997.)